Acta Universitatis Sapientiae
Electrical and Mechanical Engineering, 16 (2024) 96–109

DOI: 10.47745/auseme-2024-0009

The use of WAM Systems for Determining the Ampacity of Overhead Power Lines

František MARGITA[1], Ľubomír BEŇA[2]

[1] Department of Electric Power Engineering,
Faculty of Electrical Engineering and Informatics,
Technical University of Košice,
e-mail: frantisek.margita@tuke.sk
[2] Department of Electric Power Engineering,
Faculty of Electrical Engineering and Informatics,
Technical University of Košice,
e-mail: lubomir.bena@tuke.sk

Manuscript received April 19, 2024; revised October 24, 2024

Abstract: This study expands upon previous research by focusing on determining the dynamic thermal rating (DLR) of a specific overhead transmission line. It utilizes real-time data from WAMS (Wide Area Measurement Systems), specifically using PMUs (Phasor Measurement Units). The paper presents a comprehensive overview of thermal evaluations, which are categorized into dynamic (including direct, indirect, transient, and steady state) and static (conventional) rating. Furthermore, the article examines standards that outline principles, technologies, and algorithms for estimating conductor temperature.

Keywords: ACSR, CIGRE 601, PMU, thermal rating, WAMS.

1. Introduction

The ampacity of overhead transmission lines refers to the maximum electrical current they can sustain without compromising their electrical and mechanical integrity. ACSR (Aluminium-conductor steel-reinforced cable) conductors, with aluminum as the main material, are widely used in these lines. Manufacturers specify a maximum operating temperature typically between 90 and110°C. Exceeding this can make the material brittle, reducing its lifespan. Overloading electrical conductors is a common concern in many studies, impacting transmission capacity due to current overload issues [1], [2], [3].

It's crucial to avoid exceeding maximum extension or sag of overhead transmission lines to maintain safe distances from the ground, nearby objects, or other conductors below. Nominal values assigned during design phase set

limits on energy transmission to ensure material strength remains intact. Standards specify minimum safe conductor heights for different conditions, prioritizing reliability even under critical circumstances. Factors influencing line ampacity are illustrated in *Fig. 1* [4].

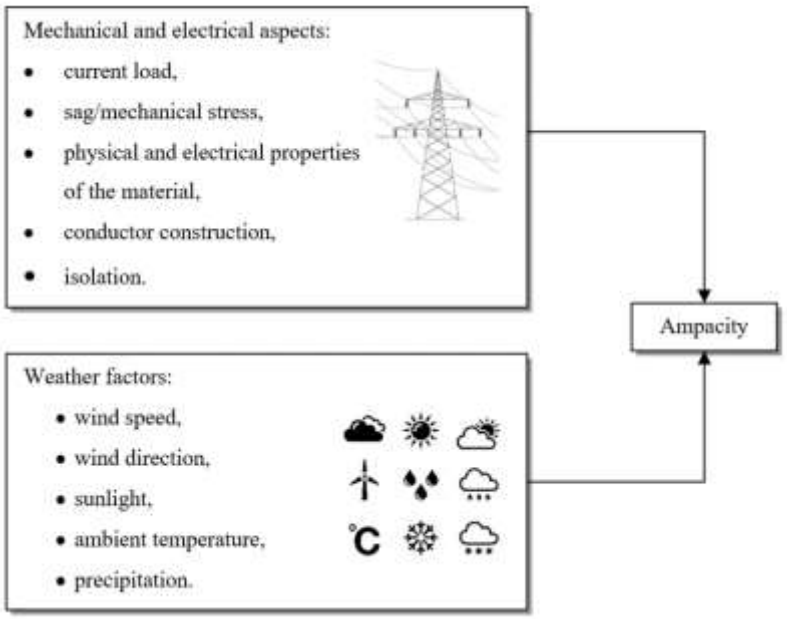

Figure 1: Factors affecting the ampacity of a conductor

2. Evaluation of thermal performance in overhead electrical lines

Ampacity determination involves two main approaches: static and dynamic. Static ampacity, or SLR, uses a probabilistic method, whereas dynamic ampacity, or DLR, is deterministic. DLR methods can be direct or indirect. Long line ampacity often relies on stability limits or voltage constraints, whereas short lines are limited by temperature [5].

A. Static line rating

In SLR, electrical grids assume constant conductor ampacity, regardless of season, with a conservative estimate focusing on theoretical rather than actual values [6]. SLR is computed utilizing a thermal model that relies on the thermal equilibrium of the bare conductor, assuming low perpendicular wind speeds (e.g., 0.5 m/s), seasonal air temperatures nearing peak values (e.g., 35 C or higher in

summer), and full solar heating (e.g., 1000 W/m^2), as outlined in CIGRE Technical Brochure 299 [7].

Meteorological conditions for SLR assessment can vary depending on the region's environment and energy companies' risk tolerance. Each transmission line may have different standard thermal ratings, including normal (continuous), long-term emergency, and short-term emergency ratings [8].

B. Dynamic line rating

DLR adjusts ampacity in real-time to match environmental changes, aiming to maximize current loading. Thermal ampacity of overhead lines fluctuates due to heating and cooling processes. Cooling effects like wind or lower temperatures can increase thermal ampacity, allowing for greater power transmission [4].

C. Indirect dynamic line rating

In DLR, transmission line ampacity dynamically adjusts based on environmental factors like ambient temperature, wind speed, solar radiation, etc. Indirect methods, known as weather-dependent line rating, use meteorological data collected along the line for evaluation. This includes inputs from weather sensors positioned along the line to assess the conductor's thermal balance equation, forming the basis for computations in DLR systems. [5].

D. Direct dynamic line rating

The direct method of DLR involves measuring electrical line properties like conductor temperature, mechanical stress, and sag. Additional data from a weather monitoring system is typically included in line evaluation. Various approaches have been proposed for estimating DLR of overhead transmission lines [5].

E. Steady-state dynamic line rating

The temperature of the conductor will stabilize at different values depending on the current. Therefore, the steady-state dynamic ampacity refers to the current level at which the conductor temperature reaches a stable equilibrium. This calculation deals with the stable temperature of the conductor before or after a transient event caused by parameter changes. The steady-state solution aims to find the stable conductor temperature with a known current and constant climate conditions [9].

F. Transient dynamic line rating

A conductor with a specified thermal ampacity can handle short-term current overload to avoid exceeding the maximum allowed temperature. This temporary overload is called transient dynamic ampacity and is limited in duration. This approach focuses on tracking changes in conductor temperature over time, accounting for variations in operating factors like climate conditions and current flow [9].

3. Thermal assessments of overhead electrical lines constructed in compliance with specified standards

CIGRE and IEEE offer guidelines for predicting ampacity and conductor temperature. Both methods assess thermal equilibrium considering factors like load and environmental conditions, focusing on heat absorption and dissipation in the conductor [10].

The initial CIGRE method computes conductor temperature in steady-state (1), while the following one employs dynamic equilibrium, considering the conductor's thermal inertia (2) [10]:

$$P_c + P_r = P_S + P_j + P_m, \tag{1}$$

where:

- P_c represents specific cooling power due to convection (W/m);
- P_r represents specific cooling power due to radiation to the surroundings (W/m);
- P_S represents specific heating power due to solar radiation (W/m);
- P_j represents specific heating power due to Joule effect (W/m);
- P_m represents the specific magnetic heating power in a conductor, caused by the interaction of the current with the magnetic field it generates, this results in additional resistive losses, particularly in steel-cored conductors like ACSR, due to effects such as the transformer effect and current redistribution in the conductor layers (W/m).

When considering the thermal inertia of the conductor, the following dynamic thermal balance (2) is used instead of the equation (1) [10]:

$$m \cdot c \cdot \frac{\mathrm{d}T_c}{\mathrm{d}t} = P_s + P_j + P_m - P_c - P_r, \tag{2}$$

where:

- m is the mass per unit length of the conductor (kg/m);
- c is the specific heat capacity of the conductor (J/(kg·K));
- T_c is the temperature of the conductor (°C).

The thermal balance at steady-state, according to IEEE Standard 738, is expressed by equation [11]:

$$P_r + P_c = P_S + P_J, \tag{3}$$

where [11]:

- P_r represents specific cooling power due to radiation to the surroundings (W/m);
- P_c represents specific cooling power due to convection (W/m);
- P_S represents specific heating power due to solar radiation (W/m);
- P_J represents specific heating power due to the Joule effect (W/m).

The IEEE method refines the heat balance calculation by removing terms that contribute negligibly to the determination of ampacity ratings. One such term is magnetic heating, which is excluded because its effect is typically minimal in most practical scenarios. Hence, the thermal balance equation (3) can be visually illustrated in *Fig.2* [11].

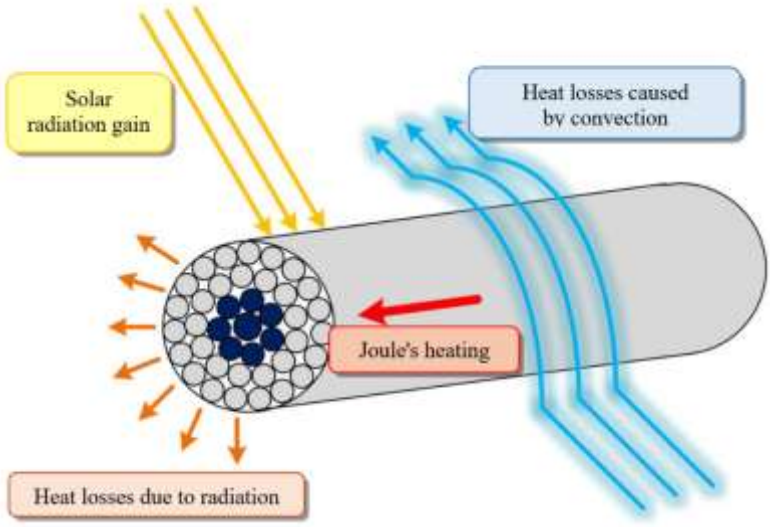

Figure 2: The thermal equilibrium of an overhead conductor as per IEEE 738

4. Tracking operational parameters through WAMS

Rising electricity consumption and energy system changes pose new challenges for operation and monitoring. SCADA alone isn't enough for ensuring system security and stability. It can't measure data from all buses simultaneously and lacks sufficient sampling frequency for some applications, resulting in inaccuracies in representing energy system dynamics [12].

New measurement technologies enable energy systems to autonomously analyze and adjust transmission capacities, potentially leveraging WAMS for optimal performance. This influences overhead lines by controlling temperatures and facilitating more flexible energy transfer [13].

WAMS improves energy system monitoring by addressing SCADA system limitations. Its main component, PMUs handles data collection, transmission, and analysis. WAMS receives data via high-speed links, processes it, extracts insights, and makes decisions to enhance system performance [12].

Fig. 3 represents the basic structure of WAMS. The WAMS structure includes the following infrastructures [12]:

1. PMU, strategically installed in the grid;
2. synchronization system, providing a concurrent image of system variables, event consequences, and operating state – synchronizing PMU sampling frequency/time for data collection and transmission;
3. data communication system, ensuring speed, reliability, and security for transmission;
4. data collection and analysis center, containing qualified software for data analysis.

Phasor data enables instant determination of energy flow in lines and assessment of their loading status. Implementing PMUs allows for real-time load determination based on actual current and weather conditions, enabling increased power transmission under specific requirements. DLR methods can be achieved in two ways [12]:

1. Based on climatic conditions such as temperature, solar radiation, and wind speed, as well as data about conductors;
2. A method to calculate DLR current using only voltage and current measurements from both ends of the line, without external ambient inputs, by estimating instantaneous temperature from line parameter variations. Steady-state conductor temperature is determined, the rated current is then derived via curve fitting of dissipated power against conductor current.

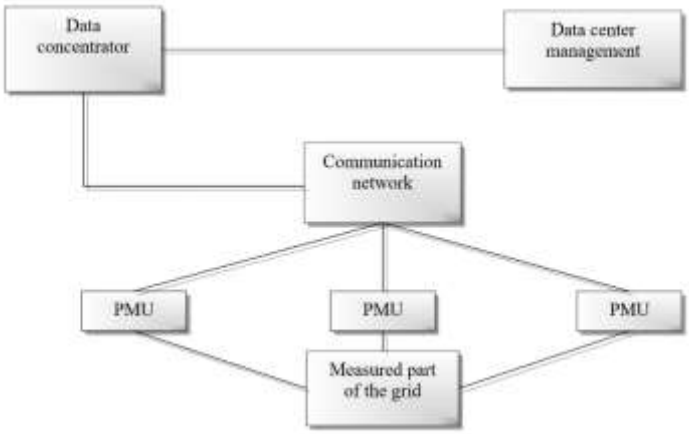

Figure 3: Principle diagram of WAMS

5. Design and practical implementation of the solution of the thermal model of the conductor

Generally, there are three models of the overhead lines: electrical, thermal, and mechanical. Despite being influenced by external variables, they also correlate with each other, as shown in *Fig. 4* [14], [15].

We begin by considering an equivalent Π circuit for the transmission overhead line. *Fig. 5* depicts the schematic diagram with voltage and current specifications. Here, the longitudinal impedance is concentrated between the line's start and end, whereas the transverse admittance is evenly divided at both ends [16], [17], [18].

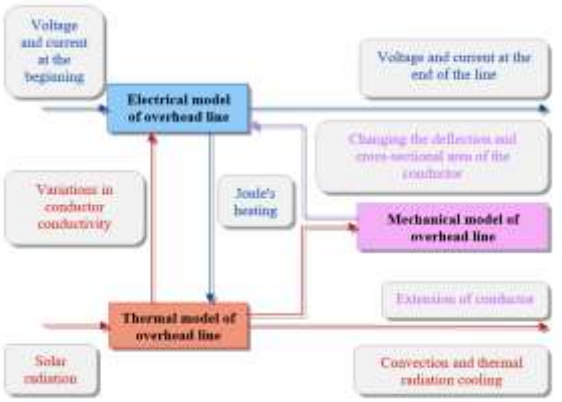

Figure 4: Models of the overhead transmission lines

As described in [17], the following parameters are used:

- $\underline{V}_1, \underline{V}_2$ represent the positive sequence voltage phasor at PMU bus 1 and 2,
- $\underline{I}_1, \underline{I}_2$ represent the positive sequence current phasor at PMU bus 1 and 2,
- $\underline{Z}$ represents the longitudinal impedance (Ω),
- $\underline{Y}_1, \underline{Y}_2$ represents the transverse admittance (S).

The studied phase conductor in Slovakia is the commonly used 352-AL1/59-ST1A conductor, with its basic parameters listed in *Table 1* [19].

According to the CIGRE Technical Brochure 601, the influence of magnetic heating can be disregarded because the 352-AL1/59-ST1A conductor contains two aluminum layers. This implies that in such a case, the effect of magnetic heating is negligible.

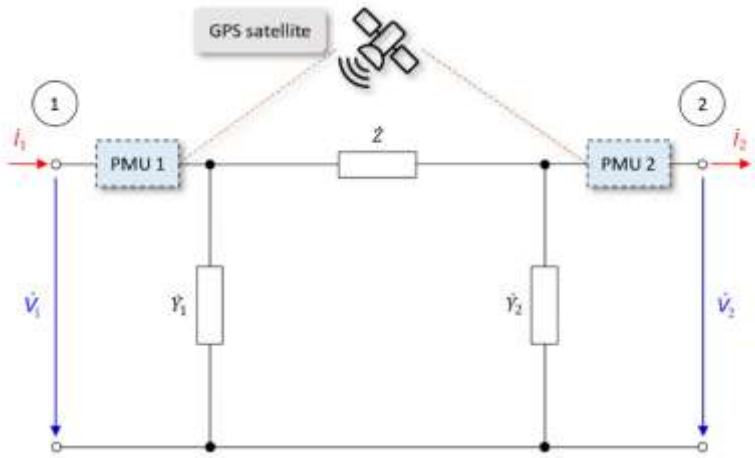

Figure 5: Equivalent circuit diagram of a transmission line using a Π-section grid

The data analyzed in this article was provided by SEPS (Slovenská elektrizačná prenosová sústava, a.s.). The data were collected from two phasor measurement units deployed at different locations within the transmission power system. PMU No. 1 was located at substation RSOB-V427-PMU1, whereas PMU No. 2 was located at substation MOLD-V427-PMU1. The PMUs were synchronized with GPS and sampled voltage and current phasors at a frequency of 1 sample per second. PMUs directly measure the phase angle ($\theta_{U1}, \theta_{U2}, \theta_{I1}, \theta_{I2}$) of voltage and current, offering real-time visibility of their phases. As a result, phases can be determined using time-synchronized voltage phase angle measurements.

The data were collected on November 25, 2021. The output after basic data processing is visualized in *Table 2* and *Table 3*.

Table 1: The technical specification of conductor 352-AL1/59-ST1A (350 ACSR 6)

Type of conductor	Conductor diameter (mm)	Diameter of the aluminum wire in the aluminum conductor (mm)	Electrical resistance of the conductor (Ω/km)	Thermal coefficient of resistance (K^{-1})	The absorptivity of the surface of the conductor (–)	Emissivity coefficient of conductor surface (–)
352-AL1/59-ST1A	26.50	4.00	0.0816	$4.03 \cdot 10^{-3}$	0.50	0.50

Table 2: Data sample obtained from PMU station RSOB-V427-PMU1

Time – (CET)	f	A_{U1} **(V)**	θ_{U1} **(°)**	A_{I1} **(A)**	θ_{I1} **(°)**
0:00:00	49.9833	414574	100	455	111
0:00:01	49.9804	414557	94	455	104
0:00:02	49.9786	414378	86	455	97
0:00:03	49.9764	414152	78	460	89
0:00:04	49.9744	414109	69	463	80

Table 3: Data sample obtained from PMU station MOLD-V427-PMU1

Time – (CET)	f	A_{U1} **(V)**	θ_{U1} **(°)**	A_{I1} **(A)**	θ_{I1} **(°)**
0:00:00	49.9833	412863	103	470	-58
0:00:01	49.9804	412815	96	469	-65
0:00:02	49.9786	412637	89	470	-72
0:00:03	49.9764	412405	81	475	-80
0:00:04	49.9744	412380	72	477	-89

The temperature of the conductor can be monitored through insights from the electrical model of the overhead transmission line (*Fig. 5*). PMUs installed at

both terminals enable obtaining phase currents and voltages from both ends of the transmission system. Telegrapher's equations can be used to explain the relationship between the positive sequence current and voltage signals [14]:

$$\underline{V}_1 = \frac{\underline{V}_2 - \underline{I}_2 \cdot \underline{Z}_\mathrm{c}(T_\mathrm{c})}{2} \mathrm{e}^{\dot{\gamma}(T_\mathrm{c}) \cdot l(T_\mathrm{c})} + \frac{\underline{V}_2 + \underline{I}_2 \cdot \underline{Z}_\mathrm{c}(T_\mathrm{c})}{2} \mathrm{e}^{-\dot{\gamma}(T_\mathrm{c}) \cdot l(T_\mathrm{c})}, \tag{4}$$

$$\underline{I}_1 = \frac{\underline{V}_2 / \underline{Z}_\mathrm{c}(T_\mathrm{c}) - \underline{I}_2}{2} \mathrm{e}^{\dot{\gamma}(T_\mathrm{c}) l(T_\mathrm{c})} - \frac{\underline{V}_2 / \underline{Z}_\mathrm{c}(T_\mathrm{c}) + \underline{I}_2}{2} \mathrm{e}^{-\dot{\gamma}(T_\mathrm{c}) \cdot l(T_\mathrm{c})}, \tag{5}$$

At the given conductor temperature T_c [15, 16]:

- $\underline{Z}_\mathrm{c}(T_\mathrm{c})$ represents the wave impedance of the conductor (Ω);
- $\underline{\gamma}(T_\mathrm{c})$ represents the wave propagation coefficient (1/km);
- $l(T_\mathrm{c})$ represents the length of the transmission line (km).

After deriving the telegraph equations (4) and (5), it is possible to find formulas for the variables $\underline{Z}_\mathrm{c}(T_\mathrm{c})$ and $\underline{\gamma}(T_\mathrm{c}) \cdot l(T_\mathrm{c})$, [20]:

$$\underline{Z}_\mathrm{c}(T_\mathrm{c}) = \sqrt{\frac{\underline{V}_1^2 - \underline{V}_2^2}{\underline{I}_1^2 - \underline{I}_2^2}}, \tag{6}$$

$$l(T_\mathrm{V}) \cdot \dot{\gamma}(T_\mathrm{V}) = \ln\left(\frac{\dot{V}_1 + \dot{Z}_\mathrm{V}(T_\mathrm{V}) \dot{I}_1}{\dot{V}_2 - \dot{Z}_\mathrm{V}(T_\mathrm{V}) \dot{I}_2} \right). \tag{7}$$

Equations (6) and (7) are used to calculate the series impedance and resistance of the line [20]. The average value of the series impedance is 28.897 Ω:

$$\underline{Z}(T_\mathrm{c}) = \underline{Z}_\mathrm{c}(T_\mathrm{c}) \cdot \underline{\gamma}(T_\mathrm{c}) \cdot l(T_\mathrm{c}), \tag{8}$$

$$R_\mathrm{AC}(T_\mathrm{c}) = \mathrm{Re}\left(\underline{Z}(T_\mathrm{c}) \right). \tag{9}$$

The actual temperature of the conductor, and thus its resistance, which changes linearly with temperature, is significantly and complexly dependent on its load current and the prevailing meteorological conditions on the line. The resistance of the series line can also be expressed relative to its reference value, as indicated below [20], [21]:

$$R_\mathrm{AC}(T_\mathrm{c}) = R_\mathrm{REF} \cdot \left(1 + \beta \cdot (T_\mathrm{c} - T_\mathrm{REF}) \right), \tag{10}$$

represented by variables [22]:

1. R_{AC} series AC (alternating current) resistance of the conductor at the given conductor temperature (Ω/m),
2. R_{REF} series AC resistance of the conductor, including skin effect, at the reference temperature, i.e., 20 °C (Ω/m),
3. β temperature coefficient of the conductor's resistance ($1/K^{-1}$),
4. T_c conductor temperature (°C),
5. T_{REF} reference conductor temperature, i.e., 20 °C.

Some ACSR conductors, such as those used in other countries, may have both the DC resistance per unit length at 20 °C and the AC resistance per unit length at 25 °C and 75 °C specified, such as the Drake conductor [9].

Finally, by modifying equation (10) for the series resistance of the conductor at a given temperature, the conductor temperature is determined by the relationship [21], [23]:

$$T_c = T_{REF} + \left[\frac{R_{AC}(T_c)}{R_{REF}} - 1 \right] \cdot \beta^{-1}. \tag{11}$$

The algorithm's key challenge lies in selecting T_{REF}, R_{AC}, and β, which directly affect conductor temperature accuracy. β, the temperature coefficient of the conductor's resistance, is typically obtained from literature. R_{AC} can be calculated using established methods or estimated using PMU data if the conductor length at T_{REF} is known. R_{REF} aids in calculating the AC resistance of the series transmission line per unit length [21].

Accuracy of this method depends heavily on the precision of voltage and current transformers, as discussed in [24]. Voltage transformers usually have a consistent level of inaccuracy, while current transformers can introduce significant errors, especially at low currents. Error correction methods, as discussed in [21], can be applied to mitigate these issues.

Authors [9], [22], and manuals (Stredoslovenská energetika, elektrika.cz) offer varied values for R_{REF} in the conductor's technical specification. Even a slight deviation can greatly affect the algorithm. As a heuristic approach, we considered R_{REF} = 0.0085 Ω/km in the algorithm. *Fig. 6* depicts the temperature changes in the conductor over time (red line), calculated from PMU data, with load conditions set to I_1 (blue line).

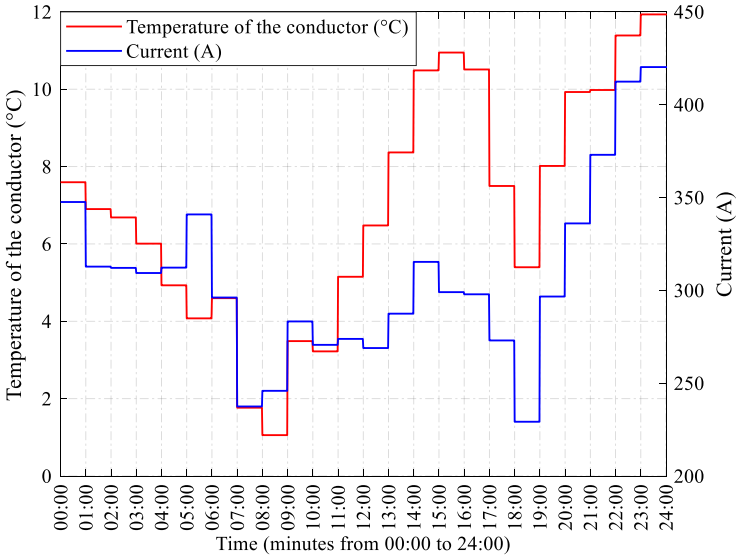

Figure 6: Conductor temperature at AC series line resistance at reference value R_{ref} based on equation (11)

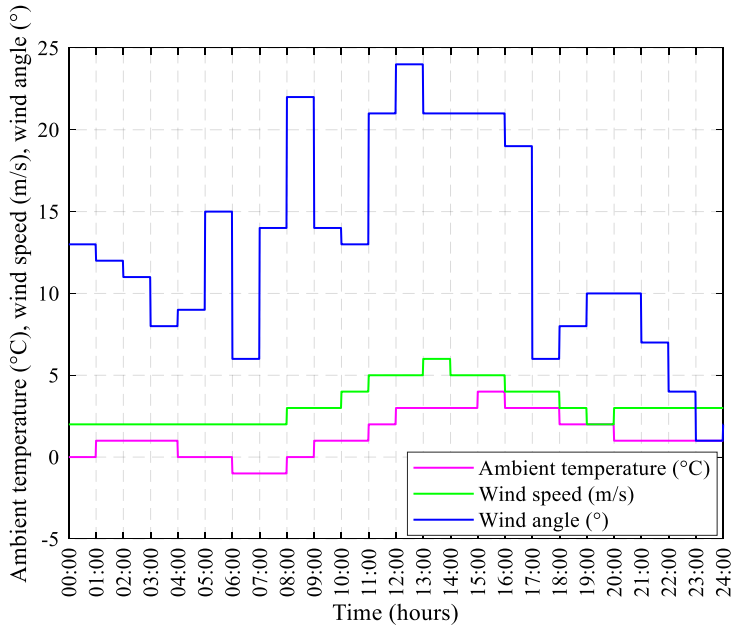

Figure 7: Meteorological conditions for the given measurement day in the transmission line region

Conclusion

In the study conducted, the focus was on examining ACSR conductor temperatures in overhead transmission lines, emphasizing the critical importance of adhering to specified temperature limits for maintaining material integrity. The significance of adhering to ampacity and sag constraints for ensuring line safety and reliability was emphasized.

Standards established by organizations such as CIGRE and IEEE were highlighted for estimating ampacity and conductor temperature. These standards employ heat balance equations that consider loading and environmental factors. Both static and dynamic approaches to ampacity determination were discussed, as they are crucial for ensuring safe line operation.

The study also delved into the role of WAMS in conductor temperature calculation and ampacity assessment. By utilizing PMU technology, WAMS enables efficient calculation of conductor temperature, surpassing the limitations of SCADA systems for informed decision-making.

Through the infrastructure provided by WAMS, conductor temperature can be computed without the need for external devices, ensuring real-time monitoring and accurate data for line optimization. The ability to calculate temperature at one-second intervals allows for timely monitoring of line conditions, which is essential for achieving optimal operation.

Acknowledgements

This work was supported by the Slovak Research and Development Agency under contracts No. APVV-19-0576 and APVV-21-0312.

References

[1] Beňa, Ľ., Kolcun, M., Medveď, D., Pavlík, M., Čonka, Z., Király, J., "The influence of climatic conditions on the dynamic ampacity of external lines", *Elektroenergetika*, vol. 15, no. 2, pp. 47, 2022.

[2] Kladar, D., "Dynamic Line Rating in the world – Overview", 2014.

[3] Pijarski, P., and Kacejko, P., "Elimination of Line Overloads in a Power System Saturated with Renewable Energy Sources", *Energies*, vol. 16, no. 9, pp. 3751, 2023, DOI: 10.3390/en16093751.

[4] IRENA, "System Operation: Innovation Landscape Briefs", 2020, pp. 1–20.

[5] Karimi, S., Musilek, P., Knight, A. M., "Dynamic thermal rating of transmission lines: A review", *Renewable and Sustainable Energy Reviews*, vol. 91, pp. 600-612, 2018, DOI: 10.1016/j.rser.2018.04.001.

[6] Simms, M., Meegahapola, L., "Comparative analysis of dynamic line rating models and feasibility to minimise energy losses in wind rich power networks", *Energy Conversion and Management*, vol. 75, pp. 11–20, 2013, DOI: 10.1016/j.enconman.2013.06.003.

[7] Working Group B2.43, “Guide for thermal rating calculation of overhead lines, Technical Brochure 601”, 2014.
[8] Douglass, D. A., et al., “A Review of Dynamic Thermal Line Rating Methods with Forecasting”, *IEEE Transactions on Power Delivery*, vol. 34, no. 6, pp. 2100–2109, 2019, DOI: 10.1109/TPWRD.2019.2932054.
[9] Margitová, A., “Increasing the transmission capacity of external power lines by calculating the dynamic ampacity”, PhD Thesis, TUKE, Košice, 2021.
[10] Arroyo, A., Castro, P. Martinez, R. Manana, M. Madrazo, A. Lecuna, R. Gonzalez, A., “Comparison between IEEE and CIGRE Thermal Behaviour Standards and Measured Temperature on a 132-kV Overhead Power Line,” *Energies*, vol. 8, no. 12, pp. 13660–13671, 2015, DOI: 10.3390/en81212391.
[11] Karunarathne, E., Wijethunge, A., Ekanayake, J., “Enhancing PV Hosting Capacity Using Voltage Control and Employing Dynamic Line Rating”, *Energies*, vol. 15, p. 134, 2022, DOI: 10.3390/en15010134.
[12] Kacejko, P., Pijarski, P., “Dynamic fitting of generation level to thermal capacity of overhead lines”, *Przeglad Elektrotechniczny*, vol. 84, pp. 80–83, 2008.
[13] Bashian, A., Assili, M., Anvari-Moghaddam, A., Catalão, J.P.S., “Optimal Design of a Wide Area Measurement System Using Hybrid Wireless Sensors and Phasor Measurement Units”, *Electronics*, vol. 8, p. 1085, 2019, DOI: 10.3390/electronics8101085.
[14] Mai, R., Fu, L., Xu, HaiBo, “Dynamic Line Rating estimator with synchronized phasor measurement”, *International Conference on Advanced Power System Automation and Protection*, Beijing, China, pp. 940–945, 2011, DOI: 10.1109/APAP.2011.6180545.
[15] Giannuzzi, G. M., Pisani, C., Vaccaro, A., Villacci, D., “Overhead transmission lines dynamic line rating estimation in WAMS environments”, *International Conference on Clean Electrical Power (ICCEP)*, Taormina, Italy, pp. 165–169, 2015, DOI: 10.1109/ICCEP.2015.7177618.
[16] Štieberová, N., Beňa, L., Margitová, A., Kanálik, M., “Calculation of parameters related to the dynamic ampacity of external lines”, *Electrical Engineering and Informatics XI*, vol. 11, no. 1, pp. 380–385, 2020.
[17] Kubek, P., Siwy, E., “Analysis methods of HTLS conductors in terms of mechanical and thermal criteria”, *Acta Energetica Power Engineering Quarterly*, vol. 1, no. 14, pp. 75-82, 2013, DOI: 10.12736/issn.2300–3022.2013107.
[18] Pavlinić, A., Komen, V., “Direct monitoring methods of overhead line conductor temperature”, *Engineering Review*, vol. 37, pp. 134–146, 2017.
[19] Kanalik, M., Margitová, A., Beňa, L., “Temperature calculation of overhead power line conductors based on CIGRE Technical Brochure 601 in Slovakia”, *Electrical Engineering*, vol. 101, 2019, DOI: 10.1007/s00202-019-00831-8.
[20] Popelka, A., Jurik, D., Marvan, P., “Actual line ampacity rating using PMU”, *CIRED*, Frankfurt, Germany, pp. 1–4, 2011.